RSC Advances

PAPER

View Article Online
View Journal | View Issue



Cite this: RSC Adv., 2015, 5, 38152

# Single-step label-free hepatitis B virus detection by a piezoelectric biosensor†

Nicoletta Giamblanco,*[a] Sabrina Conoci,*[b] Dario Russo[c] and Giovanni Marletta[a]

Received 25th February 2015
Accepted 14th April 2015

DOI: 10.1039/c5ra03467a

www.rsc.org/advances

In this paper we describe a single step and label free method to selectively detect the HVB genome based on hybridization with simple linear ssDNA probes immobilized on the Au surfaces of a QCM resonator. It has been proved that selective sensing ability is obtained for a large DNA target, constituted by an HBV clone of 7 kbps through a proper optimization of the probe density. Actually, with a probe density of $\sim 4.0 \times 10^{12}$ molecules per $cm^2$ we were able to detect fmol $cm^{-2}$ of HBV target, without using any amplification steps or labelling method. The results presented herein pave the way to the development of an easy to use and portable PoC sensor device for direct and fast HBV detection.



## Introduction

The development of nucleic acid biosensors has received increasing attention over the last decade, due to the importance of gene analysis[1] in clinical diagnostics and forensic studies.[2] In this context, most of the consolidated nucleic acid detection methods are time consuming and expensive. Consequently, there is a high demand for accurate biosensors with rapid detection systems in a portable Point-of-Care (PoC) format.

Particularly, for hepatitis B virus (HBV) detection, there is huge request to detect and monitor at early stage of infection since it is one of the major health problems worldwide leading to chronic hepatitis, cirrhosis and primarily liver cancer.[3,4]

The hepatitis B virus (HBV) is a mostly double-stranded DNA virus in the Hepadnaviridae family. The HBV virion genome is circular and approximately 3.2 kb in size and consists of DNA that is mostly double stranded. It has compact organization, with four overlapping reading frames running in one direction and no noncoding regions.[5]

Currently, the most commonly used clinical diagnostic methods for HBV detection are based on immunoassay and polymerase chain reaction (PCR). Immunoassays present a good selectivity and achieve 100% accuracy, but they do not provide quantitative results and the detection is limited by serological response.[6] On the other hands, PCR, that is traditionally the clinical standard technique to quantitatively identify HBV infection, requires complex and high cost instrumentation.[7]

DNA biosensors based on nucleic acids hybridization are currently under intense investigation owing to their increasing importance in the diagnosis of diseases, with low cost and low power requirements.[8–10]

Among the methods developed for hybridization analysis, the most attractive ones for portable PoC devices are those based on electronic detection since they offer the advantages to be easily integrated with microelectronics in miniaturized chip-based format.[11,12] Recently, increasing attention has been paid to the development of quartz crystal microbalance (QCM) biosensors due to their many merits such as compact size, high mass sensitivity, easiness to be properly functionalised in view of good specificity, low cost, label-free detection and rapid response.[13–16] Indeed, QCM detection methods require device architectures implying to immobilize specific DNA probes on Au surfaces. However, such methodologies require the control of the accessibility, in order to enable the full accessibility of the detection sites on the probe. In fact, the immobilized probe molecules may suffer a significant reduction of the appropriate exposure of the recognizing sites, when compared to the efficiency of probe-target recognition in solution. Despite extensive investigations at this regard[17–23] only a limited number of studies have been addressed to the detection of large DNA target without amplification.[24,25]

Accordingly, the performances of QCM-based biosensor devices (*i.e.* specificity, sensitivity and reproducibility) are supposed to strictly depend on the control of both homogeneity and structural features of the immobilized DNA probes, respectively involving packing density and molecular conformation.[26–29] One of the approach to improve biosensor ability and overcome the limitations in the case of large DNA target recognition, is therefore to design devices based on complex nanoarchitectures of DNA probes[30,31] involving multistep surface chemistry.[32] Again, this would represent a serious drawback for an industrial scale-up of the process.

[a]Laboratory for Molecular Surfaces and Nanotechnology (LAMSUN), Department of Chemical Sciences, University of Catania and CSGI, 95125 Catania, Italy. E-mail: n.giamblanco@unict.it

[b]STMicroelectronics, Stradale Primosole 50, 95121 Catania, Italy. E-mail: sabrina.conoci@st.com

[c]Clonit Srl, Via Bernardo Quaranta 57, 20139 Milano MI, Italy

† Electronic supplementary information (ESI) available. See DOI: 10.1039/c5ra03467a

In order to face the problems described above, in this paper we describe a single step and label free method to perform gene analysis, showing its application, as a model system, to the selective detection of HVB genome based on hybridization with simple linear ssDNA probes immobilized on Au surfaces of QCM resonator. In particular, it is shown that fast and selective sensing ability is obtained for large DNA target, constituted by HBV clone of 7 kbps through a proper optimization of the probe density. The results presented herein are very promising for the development of an easy-to-use, portable PoC sensors device for direct and fast HBV detection.

# Experimental

## 2.1 Materials and methods

Thiolated oligonucleotides probes HBS-F (henceforth indicated as P1) and HBS-R (henceforth indicated as P2) (20, 21 nts) were purchased from Eurofins MWG Operon and were prepared with concentration range 0.08–38.8 μM in ultrapure water (DNase and RNase-free, Gibco). The ultrapure water osmolality is certified to be 1.0 mOsm $kg^{-1}$ with pH 6.0.

Stock solutions of hepatitis B virus (HBV) clone complete genome (T-clone) (ref. 05960467, consisting in HBV genome 3.2 kbps and a plasmid PBR322 vector 3.8 kbps) in TE (Tris 10 mM, EDTA 1 mM, pH = 8), R-clone (ref. RT 50, consisting of Factor V of Leiden of 6062 kbps) in TE (Tris 10 mM, EDTA 1 mM, pH = 8) were provided by Clonit. These were diluted at concentration of 370 pg in ultrapure water (pH = 8.1 ± 0.2). Both these solutions (T-clone and R-clone) were denatured at 95 degrees for 5′ and immediately immersed in ice bath before use. The recognition site on hepatitis B-virus for ssDNA probe sequences P1 and P2 are located at the core protein coded for by gene C (HBcAg)[33] at nucleotide position 1 (P2) and 181 (P1), respectively (Table 1).

## 2.2 Instrumentation

**2.2.1 Quartz crystal microbalance with dissipation monitoring (QCM-D).** QCM-D measurements were carried out with a Q-Sense E1 Instrument. The gold-coated QCM crystals (QSX 301) consisting of a 100 nm layer of gold with 5 nm chromium adhesion layer were purchased from Q-Sense, Inc. The substrates were cleaned by treatment of UV–$O_3$ for 20 minutes, rinsed with Millipore water and dried with $N_2$ flow. Specifically, the QCM-D experiments were carried out in two steps as follows:

(a) Probe immobilization study: it started by flowing ultrapure water solutions ($H_2O$), followed by thiolated ssDNA probes (P1 and P2) solutions at various concentrations (38.8 μM, 7.7 μM, 0.8 μM and 0.08 μM) with nuclease free water and monitoring the related frequency and dissipation changes. After that, rinsing steps are carried out to remove the excess of probe not linked to the surface.

(b) Target recognition: it started by flowing at first solution of R-clone, at a concentration of 370 pg, followed by a rinsing step, and by the subsequent injection of the specific genome target (T-clone) with a final rinsing step. Ultrapure water was used during the probe immobilization and target hybridization steps.

All measurements were performed at temperature of 25 °C. At the frequency overtones, 15 MHz, 25 MHz, 35 MHz, 45 MHz, 55 MHz and 65 MHz, the $\Delta f$ shifts and $\Delta D$ were obtained with an accuracy of ±0.2 Hz and $\pm 0.2 \times 10^{-6}$ respectively. Frequency ($\Delta f$) and dissipation ($\Delta D$) shifts were measured with respect to a baseline obtained in ultrapure water.

**2.2.2 Atomic force microscopy (AFM).** Atomic force microscopy (AFM) was employed to measure the surface morphology at nanometer scale with Multi-mode/Nanoscope IIIA Atomic Force Microscope (AFM) (VEECO, USA) in tapping mode in liquid with a standard silicon tip (40–75 kHz frequency resonance and force constant 0.58 N $m^{-1}$). The *ex situ* samples were prepared by incubating 350 μl of the ssDNA probe solutions (P1) at concentration 7.7 μM and 0.8 μM on gold substrates for 30 minutes, then rinsing with 350 μl and gently drying with $N_2$ flow. After the ssDNA incubation step, the samples were then incubated with 350 μl R-clone or T-clone solution and imaged by AFM in $H_2O$. Data were acquired on square frames having edges 500 nm. The scan rate was 1.0 Hz. Images were recorded using both height channels with 512 × 512 measurement points (pixels). Only flattening was employed to remove the background slope processed images. Measurements were made twice on different zones of each sample. The root-mean-square (RMS) surface roughness was used to quantify variations in surface elevation over different scans area.

# Results and discussion

## 3.1 Probe anchoring study

**3.1.1 Determination of DNA probe density using QCM-D.** The immobilization of two thiol-labeled ssDNA oligonucleotides P1 and P2, respectively, onto Au surfaces, have been studied *in situ* by means of QCM with dissipation monitoring (QCM-D).

Fig. 1 reports the measured real time acoustic QCM-D curves in a concentration range of 0.8–38.8 μM for the probe P1 (Fig. 1a) and probe P2 (Fig. 1b). In this range, small but detectable amounts of adsorbed probes are found; while below

Table 1 Reports the sequence, size and molecular weight (MW) of thiolated DNA P1 and P2 probes (complementary to T-clone) and genomic target (R and T-clone)

| Name | Sequences (5′ to 3′) | Size | MW (g $mol^{-1}$) |
|---|---|---|---|
| P1 | HBS-F CACATCAGGATTCCTAGGAGG | 21 nts | 6570 |
| P2 | HBS-R GGTGAGTGATTGGAGGTTGG | 20 nts | 6519 |
| T-clone | HBV | 7000 bps | $4.6 \times 10^6$ |
| R-clone | Factor V of Leiden | 6062 bps | $4.1 \times 10^6$ |

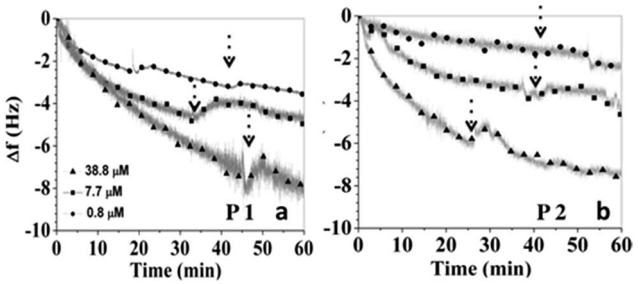


Fig. 1 Real time acoustic QCM-D curves (15 MHz). Frequency changes due to the adsorption of thiolated ssDNA probe P1 (a) and probe P2 (b) on gold are reported for solution concentrations of 38.8 μM (triangles), 7.7 μM (square), 0.8 μM (circle). Each sample addition is followed by the rinsing step indicated with arrows ($H_2O$).

the concentration of 0.8 μM (*i.e.*, 0.08 μM) no significant adsorption has been found.

According to Fig. 1, three kinetic steps can be identified: (i) probe adsorption ($\Delta f < 0$) during the surface exposure at the probe solutions; (ii) small probe desorption ($\Delta f > 0$) during the rinsing step; (iii) a further step, after rinsing, where the frequency decrease again ($\Delta f < 0$). According to literature,[34] we propose that the ssDNA molecules are anchored to the gold, *via* the thiol group, in a standing-up position. The further frequency decreasing after the rinsing step (iii) can be attributed to the adsorption of a water shell around the DNA molecules, enabling the ssDNA molecules to extend farther out into the water according to literature.[34]

Table 2 reports the averaged values measured for frequency and dissipation changes upon P1 and P2 probe adsorption. Since the measured energy dissipation $\Delta D$ is low, the Sauerbrey frequency–mass relationship can be used to calculate the amount of anchored probe.[35] According to Sauerbrey, the relationship between frequency change ($\Delta f$) and mass adsorbed ($\Delta m$) is given by $\Delta m = -\Delta f C n$, where $n$ is the harmonic number and $C$ is a experimental constant characteristic of the employed

Table 2 Frequency ($\Delta f$), dissipation shifts ($\Delta D$), number of molecules per cm$^2$ and neighbour distance ($d$) of P1 (a) and P2 (b) probes adsorbed on gold

(a) P1 probe

| [P1] conc. (μM) | $\Delta D$ ($10^{-6}$) | $\Delta f$ (Hz) | Number of molecules per cm$^2$ ($10^{12}$) | $d$ (nm) |
|---|---|---|---|---|
| 38.8 | 2.5 ± 0.3 | −7.5 ± 0.3 | 12.0 ± 0.6 | 2.9 ± 0.2 |
| 7.7 | 1.9 ± 0.2 | −5.0 ± 0.4 | 8.2 ± 0.5 | 3.5 ± 0.1 |
| 0.8 | 0.6 ± 0.2 | −2.8 ± 0.2 | 4.6 ± 0.3 | 4.7 ± 0.1 |

(b) P2 probe

| [P2] conc. (μM) | $\Delta D$ ($10^{-6}$) | $\Delta f$ (Hz) | Number of molecules per cm$^2$ ($10^{12}$) | $d$ (nm) |
|---|---|---|---|---|
| 38.8 | 2.8 ± 0.3 | −6.2 ± 0.3 | 10.0 ± 0.6 | 3.2 ± 0.2 |
| 7.7 | 1.5 ± 0.2 | −4.0 ± 0.4 | 6.4 ± 0.5 | 3.9 ± 0.1 |
| 0.8 | 0.5 ± 0.2 | −2.3 ± 0.2 | 3.7 ± 0.3 | 5.2 ± 0.1 |

sensor and equal to ~−17.7 ng cm$^{-2}$ Hz$^{-1}$ for a 5 MHz crystal. The measured averaged $\Delta f$ values for the three solution concentrations of probe P1, after the first hour of adsorption, were −7.5 ± 0.3 Hz (38.8 μM), −5.0 ± 0.4 Hz (7.7 μM) and −2.8 ± 0.2 Hz (0.8 μM), respectively corresponding to about 132.75 ± 5.3 ng cm$^{-2}$, 88.5 ± 7.8 ng cm$^{-2}$ and 49.6 ± 3.5 ng cm$^{-2}$ of absorbed mass. According to that, the respective ssDNA probe surface densities can be estimated to be 1.2 ± 0.6 × $10^{13}$ molecule per cm$^2$ (from 38.8 μM solution), 8.2 ± 0.5 × $10^{12}$ molecule per cm$^2$ (from 7.7 μM) and 4.6 ± 0.3 × $10^{12}$ molecule per cm$^2$ (from 0.8 μM) respectively. Similar results for the adsorption process with slightly lower surface density values were measured for the P2 ssDNA probe (Fig. 1b and Table 2b). The obtained surface density values are in good agreement with the literature for similar anchoring studies.[18]

**3.1.2 Binding energy from adsorption data.** The bonding between the ssDNA molecules and gold surface can be understood by deriving the binding energy from the equilibration adsorption data (reached after 1 h). In particular, the equilibrium data at the three surface densities here studied for P1 and P2 probes perfectly fit a simple Langmuir model (Fig. 2 for P1 and Fig. SI2† for P2).

The equilibrium-binding constant of the ssDNA probes on gold ($K_e$) can be calculated by eqn (1),

$$(d\Gamma(t))/dt = K_e C(1 - (\Gamma(t))/\Gamma\_max) \quad (1)$$

where $K_e = k_{ads}/k_{des}$, $d\Gamma(t)$ is the time-dependent surface density for the adsorbed molecules ($N$ molecules per cm$^2$), $\Gamma$_max is the maximum possible coverage and $C$ is the ssDNA probe concentration in solution.

The fitting of the experimental data by eqn (1), yields the following values for P1 and P2 equilibrium constants: $K_e(P1) = 6.0 \pm 1.0 \times 10^5$ M$^{-1}$ and $K_e(P2) = 4.0 \pm 0.5 \times 10^5$ M$^{-1}$.

The knowledge of the $K_e$ values, hence, allows the derivation of the free energies of adsorption of thiolated ssDNA probes P1 and P2 on gold, according to the well known relation $\Delta G = -RT \ln K_e$, where $K_e = k_{ads}/k_{des}$. In particular, from the values of $K_e$ above reported, we obtained $\Delta G_{ads}(P1) = -42.0 \pm 3.6$ kJ mol$^{-1}$ (−10.3 ± 0.9 kcal mol$^{-1}$) and $\Delta G_{ads}(P2) = -43.0 \pm 3.0$ kJ mol$^{-1}$ (−10.5 ± 0.7 kcal mol$^{-1}$). These values are in close agreement with those expected for gold/thiol bond formation

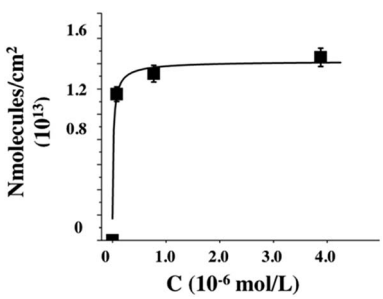


Fig. 2 Surface coverage ($N$ molecules per cm$^2$) *versus* solution concentration ($C$) of thiolated ssDNA probe (P1) after 1 hour. The correlation coefficient is $R^2 = 0.94$.

(−40 kJ mol$^{-1}$).[36] This finding supports the fact that the adsorption process essentially involves covalently bonded species, with a negligible role, if any, of non-specific interactions (*i.e.*, van der Waals, image charge, *etc.*). Moreover, it has been recently proved that the Au–S bond formation (isolated molecules) is very fast (8 s)[37] indicating that in our case, after 20 minutes (flowing time of probe surface exposure), all the thiolated probes are covalently bound.

The data reported in Fig. 2 indicate that adsorption is roughly ranging between ~3.0 × 10$^{12}$ and 1.2 × 10$^{13}$ molecules per cm$^2$, reaching a plateau value thereafter, in agreement with similar results reported in literature.[38,39]

**3.1.3 Average nearest neighbour-distance.** The average nearest neighbour distance was estimated by the equation $d = 1/\sigma^{1/2}$, where $\sigma$ is the measured probe density, under the assumption that the system consists in an hexagonal close-packed array of thiolated DNA probes. In particular, for probe P1 we have found $d = 2.9 \pm 0.2$, $d = 3.5 \pm 0.1$ nm and $4.7 \pm 0.1$ nm, respectively for the experimental densities of 1.2 ± 0.6 × 10$^{13}$, 8.2 ± 0.5 × 10$^{12}$ and 4.6 ± 0.3 × 10$^{12}$ molecules per cm$^2$. These values correspond to one ssDNA molecule per 9.0 nm$^2$, one ssDNA per 13 nm$^2$ and one ssDNA per 22 nm$^2$, respectively. A similar trend, with lower values have been found for P2 ssDNA probe, *i.e.*, $d = 3.2 \pm 0.2$ nm, $d = 3.9 \pm 0.1$ nm and $d = 5.2 \pm 0.1$ nm for the experimental density of 1.0 ± 0.6 × 10$^{13}$ molecules per cm$^2$, 6.4 ± 0.5 × 10$^{12}$ molecules per cm$^2$ and 3.7 ± 0.5 × 10$^{12}$ molecules per cm$^2$. Again, these values correspond to one ssDNA molecule per 10 nm$^2$, one ssDNA per 15 nm$^2$ and one ssDNA molecule per 27 nm$^2$, respectively. The above data suggest that the probe sequence may have a small effect on the total adsorbed mass, and, thus, on the chain density.

Also, the possible contribution of conformational and entropic forces, *i.e.*, steric hindrance factors, to the distribution of the ssDNA strands along the gold surface have been analysed. In particular, we have compared the size of the free thiolated ssDNA molecules in solution with the estimated average distance among neighbouring chemisorbed molecules on gold, for the various measured surface densities. The contour lengths of fully stretched ssDNA strands is simply $L = bN$, where $N$ is the number of bases in the strand and $b \cong 0.7$ nm is the distance between adjacent phosphorous atoms.[40] In our case $L$(P1) = 14.7 nm for $N = 21$ nts (P1 strands), and $L$(P2) = 14.0 nm for $N =$ 20 nts (P2 strands). On the other hand, the real size of the thiolated ssDNA P1 strands can be described by means of the persistence length ($l_p$), which, for the studied ssDNA strands is about 6.7 nm at the low ionic strength solutions here employed (*i.e.*, ultrapure water).[41] In this framework, the ssDNA molecules, under the condition $l_p < L$, can be represented as semi-flexible coils. In a simple bidimensional model, consisting of hexagonal close-packed arrangement,[42] a distribution of weakly stretched ssDNA brushes,[43] extending towards the solution, is therefore expected, according to well-established literature.[44]

## 3.2 Target recognition

**3.2.1 Crowding effect on target recognition.** The effect of the ssDNA probes density on the recognition efficiency and selectivity towards genomic DNA targets has been studied with respect to a specific genomic target T-clone and a non-complementary genome R-clone, both at concentration of 370 pg (denaturated at 95 °C before hybridization). In the following discussion we focus the attention to the response of P1 probe to the T and R clones, as for P2 very similar effects have been observed.

Fig. 3 shows the measured real time hybridization QCM-D curves for the three surface densities cases of P1 probe: 1.2 × 10$^{13}$ molecules per cm$^2$, 8.2 × 10$^{12}$ molecules per cm$^2$ and 4.6 × 10$^{12}$ molecules per cm$^2$. It can be noticed that the most efficient hybridization is found for the probe density surfaces of 4.6 × 10$^{12}$ molecules per cm$^2$ (the lowest here explored) while the higher surface density samples show an almost negligible hybridization capability. In particular, Fig. 3a and b show that the surfaces with highest P1 probe density (1.2 × 10$^{13}$ molecules per cm$^2$ and 8.2 × 10$^{12}$ molecules per cm$^2$) produces a small and completely reversible adsorption for both the T- and R-clones, while for the low density surfaces (*i.e.*, about 4.6 × 10$^{12}$ molecules per cm$^2$, Fig. 3c) a strongly selective and irreversible hybridization is found for T-clones, as shown by Fig. 3d, while the non-specific R-clones shows a negligible adsorption. In other words, the 4.6 × 10$^{12}$ molecules per cm$^2$ surface density samples show a dramatic increase in selective adsorption of T clone. Moreover, the low density surfaces retained about 45.0 ng cm$^{-2}$ of T-clone mass (see Table 3), roughly corresponding to 1.2 × 10$^{10}$ molecules per cm$^2$ and, in turn, to 0.02 pmol cm$^{-2}$, accordingly, the 4.6 × 10$^{12}$ molecules per cm$^2$ density surfaces may, in principle, reveal femtomolar concentrations.

As far as the P2-is concerned, the best surface probe density T-clone recognition resulted the same than for P1 ssDNA species, *i.e.*, about 4.0 × 10$^{12}$ molecules per cm$^2$, yielding a genome T-clone retained mass of 42 ng cm$^{-2}$, very close to the one measured for P1 (Fig. SI4†).

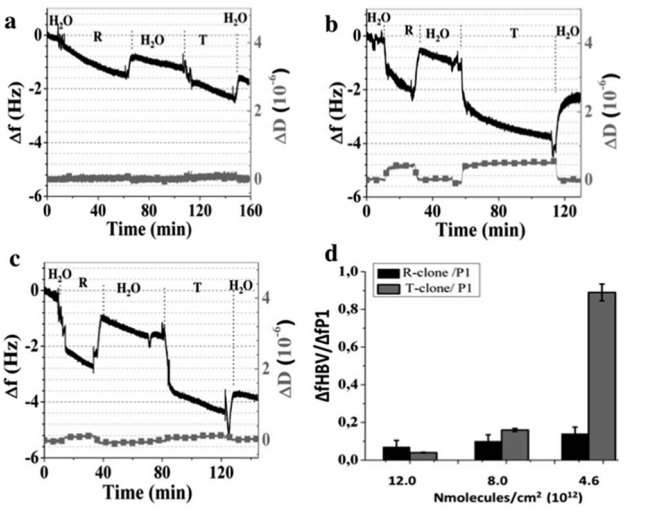


Fig. 3 QCM-D kinetic curves of non-specific R-clones onto the ssDNA probe (P1), followed by washing with $H_2O$ and then flowed with specific T-clones and a final rinsing step. The ssDNA P1 probe density are (a) 1.2 × 10$^{13}$ molecules per cm$^2$; (b) 8.2 × 10$^{12}$ molecules per cm$^2$; (c) 4.6 × 10$^{12}$ molecules per cm$^2$. Panel (d) reports the clone to probe ratios for R/P1 and T/P1 for all the investigated ssDNA surface densities.

Table 3 Frequency shifts (Hz) and $\Delta m$ (ng cm$^{-2}$) for nonspecific (R) and specific (T) clone hybridized with P1 probe at different surface density

| Probe P1 | R-clone | | T-clone | |
|---|---|---|---|---|
| $N$ molecules per cm$^2$ $10^{12}$ | $\Delta f$ (Hz) | $\Delta m$ (ng cm$^{-2}$) | $\Delta f$ (Hz) | $\Delta m$ (ng cm$^{-2}$) |
| 12.0 ± 0.6 | −0.5 ± 0.2 | 8.8 ± 3.5 | −0.3 ± 0.2 | 5.3 ± 3.5 |
| 8.2 ± 0.5 | −0.5 ± 0.2 | 8.8 ± 3.5 | −0.3 ± 0.2 | 5.3 ± 3.5 |
| 4.6 ± 0.3 | −0.4 ± 0.2 | 7.1 ± 3.5 | −2.5 ± 0.3 | 45 ± 5.3 |

It should be stressed that in this case non-specific R-clones were not adsorbed at all, indicating that neither recognition nor non-specific adsorption events occurred (see Fig. SI4†).

These findings highlight that the recognition of HBV genome is possible by a single step without requiring any amplification procedure.

**3.2.2 Topography measurement by AFM.** The recognition step is confirmed by AFM analysis. Fig. 4 shows the pictures obtained for reference gold surfaces with immobilized 8.2 × $10^{12}$ and 4.6 × $10^{12}$ P1-molecules per cm$^2$ (Fig. 4a and c), respectively. Fig. 4b and d shows the same surfaces reacted with T-clone solutions. In the case of 8.2 × $10^{12}$ P1-molecules per cm$^2$ surface, it cannot be seen any T-clone presence (Fig. 4b). On the contrary, the presence of circular HBV can be recognized on 4.6 × $10^{12}$ P1-molecules per cm$^2$ surface, supporting the occurred hybridization above described. In this case, the obtained results support the grain size analysis, suggesting that the recognition basically involves 42 ± 7.0 nm long T-clone isolated molecules with an average distance between two neighboring HBV of about 70.0 ± 8.0 nm. The number of HBV T-clone counted in the inspected AFM area (500 nm × 500 nm) is therefore about 30. By considering the P1 probe density (4.6 × $10^{12}$ molecules per cm$^2$), the theoretical P1/T-clone ratio in the inspected AFM area is about 400.

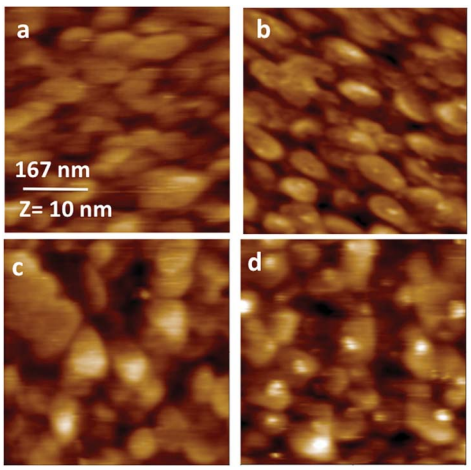


Fig. 4 Height AFM images of gold surfaces functionalized with thiolated ssDNA from 7.7 μM (a) and 0.8 μM (c) solution; AFM images of the thiolated surfaces exposed to T-clone (b) and (d).

The AFM results found a nice confirmation by comparing them to the data of surface densities for P1 and retained density of T-clone measured by QCM-D. Indeed, by calculating the hybridization HBV : P1 probes ratio, *i.e.*, the retained 1.2 × $10^{10}$ molecules per cm$^2$ HBV and the 4.6 × $10^{12}$ molecules per cm$^2$ P1 probe density, a value of about 400 : 1 is obtained as well.

**3.2.3 Kinetics of recognition and hybridization of target onto probes.** The analysis, according to a simple first-order Langmuir kinetics, of the time-dependent T-clone mass uptake for the three different probe density surfaces provide further hints on the hybridization process:[45]

$$\frac{d\sigma_T}{dt} = k_a C_T(\sigma_P - \sigma_T) - k_d\sigma_T \quad (2)$$

where $k_a$ and $k_d$ are the association and desorption rate constants, $C_T$ is the bulk concentration of HBV target, $\sigma_T$ is the surface density of hybridized molecules of target, $\sigma_P$ is the surface probe density. If target is constant as it is continuously and in excess, this can be integrated to

$$\sigma_T(t) = \sigma_T^{eq}(1 - \exp(k_{eff}t)) \quad (3)$$

where $k_{eff} = k_aC_T + k_d$ is the effective rate constant. The characteristic time scale of the reaction is given by $\tau = 1/k_{eff}$ taking into account an association rate constant, $k_a$ and a desorption constant, $k_d$.

Fig. 5 reports the kinetic curves of mass change (ng cm$^{-2}$) *vs.* $t$ (s) for the two processes: (i) target hybridization ($\Delta m > 0$) during the surface exposure at the target solution; (ii) target excess desorption ($\Delta m < 0$) during the rinsing step.

All the curves of the hybridized target mass *vs.* time can be fitted by eqn (3) with $\Delta m_{max}$ and $k_{eff}$ are the fitting parameters.

In particular, since $\tau = 1/k_{eff} = (k_aC_T + k_d)^{-1}$ and $C_T$ is the same (370 pg) for the three probe densities, $\tau_a \sim (k_aC_T)^{-1}$ and $\tau_d \sim k_d{}^{-1}$.

Accordingly, Table 4 reports the $\tau_a$ values obtained by the fitting respectively for target hybridization and target excess desorption $\tau_d$, at the three different surface densities of P1 probe.

It can be seen, again, that the values of $\tau_a \sim 210$ s are obtained for the low probe density surfaces, suggesting that for these surfaces the P1 probe molecules are more accessible than

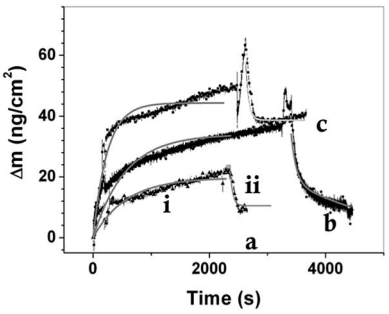


Fig. 5 Mass uptake curves *versus* time ($t$) measured by means of QCM-D technique for specific genomic T-clone onto P1-functionalized gold sensors at various probe densities including 1.2 × $10^{13}$ molecules per cm$^2$ (a), 8.2 × $10^{12}$ (b) and 4.6 × $10^{12}$ (c) molecules per cm$^2$.

Table 4 $\tau$ (s) values for specific HBV (T) clone hybridization/target excess desorption processes with P1 probe at different surface density

| Probe P1 | T-clone | |
|---|---|---|
| $N$ molecules per cm$^2$ $10^{12}$ | $\tau_a$ (s) | $\tau_d$ (s) |
| 12.0 ± 0.6 | 1601 ± 100 | 100 ± 20 |
| 8.2 ± 0.5 | 1002 ± 120 | 80 ± 10 |
| 4.6 ± 0.3 | 217 ± 20 | 65 ± 8.0 |

at higher probe density, prompting the observed faster and efficient recognition of HBV-clone molecules (T-clones). Moreover, the high $\tau_d \sim 1/k_d$ values are almost comparable to $k_aC_T$, indicating that the surface concentration of bound targets ($\sigma_T$) will be less than initial surface concentration of probes ($\sigma_P$).

## Conclusions

The data reported above confirm that there is in general a critical probe density threshold to achieve the most effective biomolecules recognition by immobilized probes. In particular, in the case of large HBV virus recognition by means of ssDNA strands as probes, the threshold turns to be about 4–5 $\times$ $10^{12}$ probes per cm$^2$. Clearly, the density threshold for different probe-target couples depends on the matching of several affinity factors, including the ones controlling the diffusion of the target molecules to the probe hybridization sites, *i.e.*, primarily the target concentration in solution and the size and conformation of the probes *vs.* the target to be recognized, as well as the probe–probe spacing. Accordingly, Scheme 1 reports the P1 inter-probe distance respectively for $1 \times 10^{13}$ molecules per cm$^2$ and $4.0 \times 10^{12}$ molecules per cm$^2$ for the anchored thiolated ssDNA strands. The scheme stresses the difficulty of the target of penetrating the probe layer if the probe densities are too high and the increased facility of clone penetration, turning in a selective recognition, for low-density surfaces.

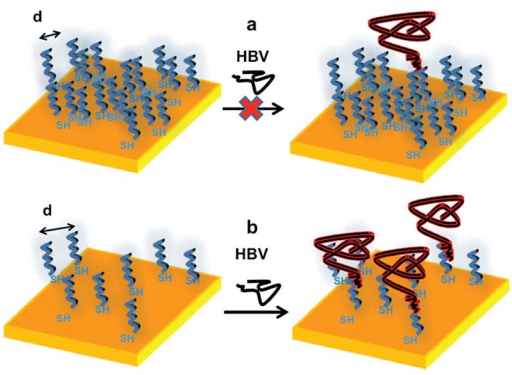


Scheme 1 Crowding effect in the organization of thiolated ssDNA strands (21 nts) on gold surfaces: (a) high probe density surfaces, with hindered HBV hybridization; (b) low probe density surfaces, allowing efficient and selective HBV recognition.

Additionally, the study revealed an important connection between the effect of ssDNA surface crowding and the kinetic step of HBV hybridization.

Indeed, to our knowledge only few literature reports are dedicated to of the study of the hybridization kinetics of ssDNA towards similar oligonucleotides,[18,46–50] so that the present paper is the first model determining how the ssDNA probe density affects the association and desorption rate with a large genome, in this case the one of HBV virus. In particular, the present study paves the way to a further work aimed to develop quantitative general models for the conception and optimization of DNA chips on new conception, taking profit of a direct and selective recognition process by means of a quartz crystal microbalance sensor, working based on a single step and label free method to selectively detect genome.

The core feature of such a class of devices is clearly based on the controlled hybridization of the target biomolecules with simple linear ssDNA probes suitably immobilized on Au surfaces of the QCM resonator.

To this purpose, the control of surface density, which determines the probe accessibility, is an essential parameter for the final properties of the device and can be quantitatively controlled. Our results show that it is possible to finely control the density and, in turn, the hybridization efficiency also for very large genomes as the one of HBV. This results in a sensitivity of fmol cm$^{-2}$, without the need of any amplification steps or labelling methods. These findings open intriguing prospects towards the fabrication of biosensors able to detect HBV virus in a single-step process.

In summary, the QCM-D biosensors have been shown to exhibit competitive sensitivity and fast response in detection of HBV virus combined with simple detection protocol and probe immobilization process. The described results, hence, prompt the development of an easy to use single-step and portable PoC sensors device for direct and fast HBV detection.

## Acknowledgements

This work has been funded by MIUR by means of the national Program PON R&C 2007–2013, project “Hyppocrates – Sviluppo di Micro e Nano-Tecnologie e Sistemi Avanzati per la Salute dell'uomo” (PON02 00355) and PRIN 2010–2011 “Metodologie chimiche innovative per biomateriali intelligenti”.

## Notes and references

1 J. Wang, *Nucleic Acids Res.*, 2000, **28**(16), 3011–3016.
2 M. Minunni, S. Tombelli, R. Scielzi, I. Mannelli, M. Mascini and C. Gaudiano, *Anal. Chim. Acta*, 2003, **481**, 55–64.
3 C. Trépo, H. L. Y. Chan and A. Lok, *Lancet*, 2014, **384**, 2053–2063.
4 R. P. Beasley, *Cancer*, 1988, **61**, 1942–1956.
5 J. H. Stares and E. G. Stares, *Viruses and Human Disease*, Academic Press, San Diego, California, 2002, p. 383.
6 A. S. F. Lok and B. J. McMahon, *Hepatology*, 2001, **34**, 1225–1241.

7 H. Huang, L. Jin, X. Yang, Q. Song, B. Zou, S. Jiang, L. Sun and G. Zhou, *Biosens. Bioelectron.*, 2013, **42**, 261–266.
8 D. Paraskevis, C. Haida, N. Tassopoulos, M. Raptopoulou, D. Tsantoulas, H. Papachristou, V. Sypsa and A. Hatzakis, *J. Virol. Methods*, 2002, **103**, 201–212.
9 W. Haasnoot, H. Gerçek, G. Cazemier and M. W. Nielen, *Anal. Chim. Acta*, 2007, **586**, 312–318.
10 D. P. Kalogianni, T. Koraki, T. K. Christopoulos and P. C. Ioannou, *Biosens. Bioelectron.*, 2006, **21**, 1069–1076.
11 T. G. Drummond, M. G. Hill and J. K. Barton, *Nat. Biotechnol.*, 2003, **21**, 1192–1199.
12 S. K. Sia and L. J. Kricka, *Lab Chip*, 2008, **8**, 1982–1983.
13 S. Conoci, A. Mascali and F. Pappalardo, *RSC Adv.*, 2014, **4**, 2845–2850.
14 C. March, J. J. Manclús, Y. Jiménez, A. Arnau and A. Montoya, *Talanta*, 2009, **78**, 827–833.
15 C. Yao, T. Zhu, J. Tang, R. Wu, Q. Chen, M. Chen, B. Zhang, J. Huang and W. Fu, *Biosens. Bioelectron.*, 2008, **23**, 879–885.
16 T. Xu, J. Miao, Z. Wang, L. Yu and C. Li, *Sens. Actuators, B*, 2011, **151**, 370–376.
17 N. Tuccitto, N. Giamblanco, S. Ghosh, V. Spmpinato, P. Labbè, P. Dumy, S. Quici, G. Marletta, E. Defrancq and A. Licciardello, *Langmuir*, 2011, **27**(14), 8595–8599.
18 G. Yang, Y. Gao, K. W. Lauren and R. M. Georgiadis, *Nucleic Acids Res.*, 2006, **34**(11), 3370–3377.
19 T. Strachan and A. P. Read, in *Human Molecular Genetics*, Wiley-Liss, New York, 2nd edn, 1999, ch. 5, Nucleic acid hybridization assays.
20 X. C. Zhou, L. Q. Huang and F. Y. Li Sam, *Biosens. Bioelectron.*, 2001, **16**, 85–96.
21 S. Yamaguchi, T. Shimomura, T. Tatsuma and N. Oyama, *Anal. Chem.*, 1993, **65**(14), 1925–1927.
22 H. Su and M. Thompson, *Biosens. Bioelectron.*, 1995, **10**(3/4), 329–340.
23 F. Caruso, H. Rodda, D. F. Furlong, K. Niikura and Y. Okahata, *Anal. Chem.*, 1997, **69**, 2043–2049.
24 C. Yao, T. Zhu, J. Tang, R. Wu, Q. Chen, M. Chen, B. Zhang, J. Huang and W. Fu, *Biosens. Bioelectron.*, 2008, **23**, 879–885.
25 X. Zhou, L. Liu, M. Hu, L. Wang and J. Hu, *J. Pharm. Biomed. Anal.*, 2002, **27**, 341–345.
26 H. Su, C. Sandra and M. Thompson, *Biosens. Bioelectron.*, 1997, **12**(3), 161–173.
27 A. W. Peterson, R. J. Heaton and R. M. Georgiadis, *Nucleic Acids Res.*, 2001, **24**, 5163–5168.
28 Y. Danfeng, K. Junyoung, Y. Fang, E. P. Nielsen, E.-K. Sinner and W. Knoll, *Biophys. J.*, 2005, **88**, 2745–2751.
29 D. Irving, P. Gong and R. Levicky, *J. Phys. Chem. B*, 2010, **114**(22), 7631–7640.
30 J. Zeng, A. Almadidy, J. Watterson and U. J. Krull, *Sens. Actuators, B*, 2003, **90**, 68–75.
31 Y. Ke, S. Lindsay, Y. Chang, Y. Liu and H. Yan, *Science*, 2008, **319**, 180–183.
32 C. Lin, Y. Liu and H. Yan, *Biochemistry*, 2009, **48**(8), 1663–1674.
33 S. Hernández, M. Venegas and R. A. Villanueva, *Genome Announcements*, 2014, **2**(5), e01075.
34 J. Mertens, C. Rogero, M. Calleja, D. Ramos, J. A. Martín-Gago, C. Briones and J. Tamayo, *Nat. Nanotechnol.*, 2008, **3**, 301–307.
35 G. Z. Sauerbrey, *Z. Phys.*, 1959, **155**, 206.
36 M. Yang and H. C. M. Chan, *Langmuir*, 1998, **14**, 6121–6129.
37 Y. Xue, X. Li, H. Li and W. Zhang, *Nat. Commun.*, 2015, **5**, 4348–4357.
38 A. Singh, S. Snyder, L. Lee, A. P. R. Johnston, F. Caruso and Y. G. Yingling, *Langmuir*, 2010, **26**, 17339–17347.
39 Z. F. Gao, J. B. Gao, L. Y. Zhou, Y. Zhang, J. C. Si, H. Q. Luo and N. B. Li, *RSC Adv.*, 2013, **3**, 12334–12340.
40 S. B. Smith, Y. J. Cui and C. Bustamante, *Science*, 1996, **271**, 795–799.
41 K. Rechendorff, G. Witz, J. Adamcik and G. Dietler, *J. Chem. Phys.*, 2009, **131**, 095103.
42 G. Doni, M. D. N. Ngavouka, A. Barducci, P. Parisse, A. De Vita, G. Scoles, L. Casalisce and G. M. Pavan, *Nanoscale*, 2013, **5**, 9988–9993.
43 B. Zhao and W. J. Brittain, *Prog. Polym. Sci.*, 2000, **25**(5), 677–710.
44 G. Wu, H. Ji, K. Hansen, T. Thundat, R. Datar, R. Cote, M. F. Hagan, A. K. Chakraborty and A. Mayumdar, *Proc. Natl. Acad. Sci. U. S. A.*, 2001, **98**, 1560–1564.
45 D. R. Purvis, D. Pollard-Knight and P. A. Lowe, in *Commercial Biosensors*, ed. G. Ramsay, Wiley-Interscience, New York, 1998, pp. 165–224.
46 B. P. Nelson, T. E. Grimsrud, M. R. Liles, R. M. Goodman and R. M. Corn, *Anal. Chem.*, 2001, **73**, 1–7.
47 A. W. Peterson, L. K. Wolf and R. M. Georgiadis, *J. Am. Chem. Soc.*, 2002, **124**, 14601–14607.
48 A. Vainrub and M. B. Pettitt, *Biopolymers*, 2003, **68**, 265–270.
49 P. W. Stevens, J. Sun and D. M. Kelso, *Anal. Biochem.*, 1999, **276**, 204–214.
50 M. F. Hagan and A. K. Chakraborty, *J. Chem. Phys.*, 2004, **120**, 4958–4968.

 